XLI CILAMCE
XLI Ibero-Latin American Congress on Computational Methods in Engineering
16-19 November, 2020 FOZ DO IGUAÇU PARANÁ - BRAZIL

Hybrid multiscale modeling of tumor growth with chemotherapeutic drug dispersion

Gustavo T. Naozuka[1], Heber L. Rocha[2], Regina C. Almeida[1]

[1]*Laboratório Nacional de Computação Científica*
Av. Getúlio Vargas, 333, 25651-075, Petrópolis/RJ, Brazil
naozuka@lncc.br, rcca@lncc.br
[2]*Department of Intelligent Systems Engineering, Indiana University*
700 N Woodlawn Ave, 47408, Bloomington/IN, USA
hlimadar@iu.edu

Abstract. Cancer is a group of diseases characterized by complex phenomena across multiple temporal and spatial scales. Comprehending its growth dynamics is a challenge and may improve the understanding of underlying mechanisms, and suggests more effective therapy protocols. In this context, mathematical and computational modeling may provide insights into tumorigenesis, cancer growth, and response to drug treatments. In this work, we develop a hybrid discrete-continuum model describing the avascular phase of cancer growth and incorporate chemotherapeutic drugs acting in different phases of the cell cycle. The growth phenomenon occurs at three scales: (i) at the tissue scale, partial differential equations model oxygen, drug, and growth factor dispersion; (ii) at the cellular scale, an agent-based model describes transitions among phenotypic states of each tumor cell and mechanical interactions among cells and the microenvironment; (iii) at the molecular level, ordinary differential equations represent signaling pathways that regulate cellular metabolism, cell cycle, and cell proliferation. Computational experiments demonstrate that the proposed modeling framework can be instrumental in the development of innovative new treatments for cancer patients.

Keywords: Cancer, Differential equations, Agent-based model, Phase-specific chemotherapeutic drug, Cell cycle

1 Introduction

The study of a complex biological phenomenon like cancer requires dealing with different interconnected spatial and temporal scales. The dispersion of oxygen and growth factors at the tissue scale, for example, directly or indirectly affects the phenomena that occur at the cellular and molecular levels. Similarly, biochemical reactions within cells impact the metabolism of cellular and tissue levels. From a modeling point of view, this multiscale nature of cancer reinforces the use of multiscale models to provide a closer representation of the real problem [1]. At various time and space scales, mathematical and computational models can be divided into continuous and discrete (based on individuals) models. Tumor continuous models allow a broader view of tumor burden growth and are generally described by differential equations. On the other hand, discrete models allow to track individual characteristics of each tumor cell and are often represented by cellular automata or agent-based models (ABMs) [2]. A model that combines both continuous and discrete approaches is called a hybrid model.

In this work, we develop a two-dimensional hybrid multiscale model that integrates features present in two tumor growth models [3, 4]. Rocha et al. [3] built a hybrid discrete-continuous model encompassing tissue, cellular, and subcellular scales. At the tissue scale, they considered the dispersion of oxygen and growth factors in the microenvironment; at the cellular level, they described the dynamics of normal and tumor cells; at the subcellular level, each tumor cell is integrated into an epidermal growth factor receptor (EGFR) signaling pathway. Powathil et al. [4] also proposed a hybrid multiscale approach. In their model, each tumor cell cycle is modeled, allowing to identify cell phases and thus to analyze the effects of cell cycle-specific chemotherapeutic drugs. Our developed model is used to perform *in silico* experiments in which we investigate the effects of two cytotoxic drugs on the behavior of tumor cells.

The remainder of the paper is organized as follows. Section 2 details the model characteristics and the resolution methods. Section 3 presents and discusses the results of the *in silico* experiments. Section 4 outlines

some final remarks and future perspectives.

2 Materials and Methods

In our model, an ABM describes the behavior and mechanical interactions among the cellular scale constituents. The agents can symbolize normal cells, tumor cells, or a pre-existing network of blood vessel cross-sections. Of note, the present contribution deals with the avascular phase of tumor development in which we assume normal cells in homeostasis. In contrast, tumor cells are differentiated into several phenotypic states, including quiescent, proliferative, hypoxic, necrotic, apoptotic, and killed by chemotherapy. At the tissue scale, the epidermal growth factor (EGF) released by quiescent cells, oxygen, and chemotherapeutic drugs released by blood vessels disperse in the microenvironment, whose concentrations are modeled by using partial differential equations (PDEs). EGF binds to the corresponding receptor (EGFR) at each cell surface and triggers a cascade of biochemical reactions within the cell. This EGFR pathway is upregulated in many cancers and is known to modulate a variety of cell responses, including cell proliferation. Oxygen, in turn, provides energy to keep cell metabolism working. Chemotherapeutic drugs are responsible for drug-induced death of part of the tumor cells. Tumor cells are also associated with a signaling pathway that governs the cell cycle. We model each signaling pathway by a system of ordinary differential equations (ODEs). Figure 1 illustrates a schematic representation of the main components of our hybrid multiscale model and their connections.

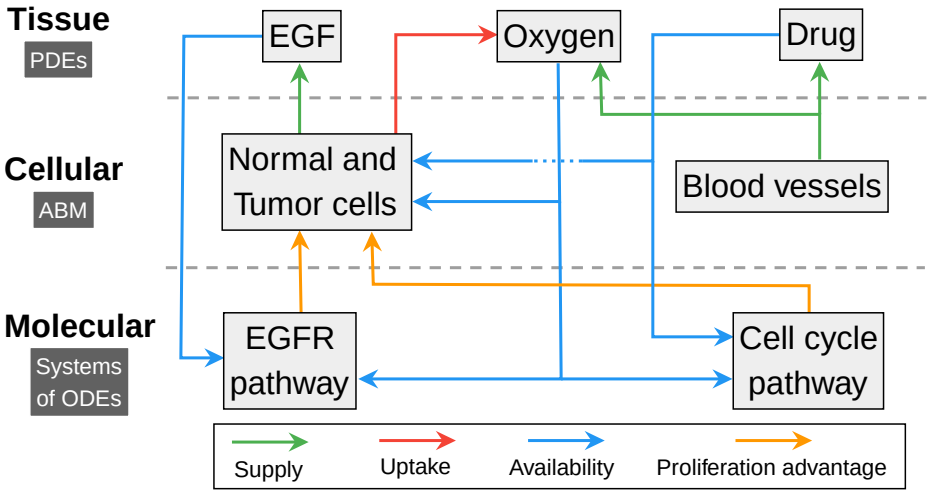

Figure 1. Schematic representation of the hybrid multiscale model developed.

2.1 The Tissue Scale

At the macroscopic scale, we consider the dispersion of EGF (released by quiescent cells), oxygen, and chemotherapeutic drug (released by blood vessels) concentrations through reaction-diffusion PDEs. The reaction terms act as connections between the cellular and tissue scales through a homogenization process [3]. Since we kept the EGF dispersion model and parameter values as described in Rocha et al. [3], we refer the reader to this paper for more information.

The dynamics of oxygen concentration ($K(x,t)$) in the tumor microenvironment is expressed by [4]:

$$\frac{\partial K(x,t)}{\partial t} = \nabla \cdot (D_K \nabla K(x,t)) + r_K - \phi_K K(x,t), \tag{1}$$

with homogeneous Neumann boundary conditions and null initial condition. In Equation (1), D_K is the diffusion coefficient, r_K is the oxygen production rate by blood vessels, and ϕ_K is the oxygen consumption rate, denoted by ϕ_{K_b}, for normal cells; or ϕ_{K_t}, for living tumor cells. As the tumor grows, there is an imbalance between oxygen production and consumption, decreasing its availability. This yields the upregulation of the hypoxia-inducible transcription factor-1 ([HIF]), which modulates the cell cycle length. Specifically, [HIF] ultimately controls oxygen availability in the cell cycle pathway (see Equation (3)), with [HIF] set equal to one where the oxygen concentration is less than a threshold $\overline{K}$, and equal to zero otherwise.

In this work, we consider possible combination of two chemotherapy medications used to treat a number of cancers: *cisplatin* (c) and *taxotere* (t). The diffusion of the i^{th} drug concentration, denoted by $C_i(x,t), i = c, t$, in

the tumor microenvironment is given by [4]:

$$\frac{\partial C_i(x,t)}{\partial t} = \nabla \cdot (D_{C_i} \nabla C_i(x,t)) + r_{C_i} - \eta_{C_i} C_i(x,t), \quad i = c, t\,, \tag{2}$$

with homogeneous Neumann boundary conditions and null initial condition. In Equation (2), D_{C_i}, r_{C_i}, and η_{C_i} are the diffusion coefficient, supply rate by blood vessels, and decay rate of the i^{th} chemotherapeutic drug. If the drug concentration uptaken by the cell is greater than a threshold ($\overline{C}$) and if the cell is in the correct phase of the cell cycle, then there is a non-zero probability that the cell will be killed by chemotherapy (see Equation (9)). The parameter values used in the dispersion models are shown in Table 1.

Table 1. Parameter values of the oxygen and chemotherapeutic drug models.

Parameter	Meaning	Value	Unit	Reference
D_K	Oxygen diffusion coefficient	4.5×10^5	$\mu\text{m}^2\text{h}^{-1}$	[4]
r_K	Oxygen production rate by blood vessels	29.52	mols h^{-1}	[4]
ϕ_{K_t}	Oxygen uptake rate by tumor cells	720.0	h^{-1}	[4]
ϕ_{K_b}	Oxygen uptake rate by healthy cells	$0.01\phi_{K_t}$	h^{-1}	[5]
$\overline{K}$	Hypoxic threshold	0.1	–	[4]
D_{C_c}	*Cisplatin* diffusion coefficient	1.71×10^5	$\mu\text{m}^2\text{h}^{-1}$	[4]
D_{C_t}	*Taxotere* diffusion coefficient	4.5×10^4	$\mu\text{m}^2\text{h}^{-1}$	[4]
r_{C_i}	Drug supply rate by blood vessels	81.281	–	[6]
η_{C_c}	*Cisplatin* decay rate	1.316	h^{-1}	[4]
η_{C_t}	*Taxotere* decay rate	0.05634	h^{-1}	[4]
$\overline{C}$	Cell death threshold	0.18	–	[6]

2.2 The Molecular Scale

At the molecular level, we model two cascades of biochemical reactions in each tumor cell: the EGFR and cell cycle pathways. The EGFR pathway is upregulated in many cancers and can be mathematically modeled by a system of 20 ODEs (see Rocha et al. [3] for a complete description). Among all the molecules involved in this process, the molecules ERK (extracellular signal-regulated kinase) and PLC_γ (phospholipase C-gamma) play fundamental roles in the cell proliferation process. If the variations in the PLC_γ and ERK concentrations along time are less and greater than two thresholds (T_{PLC} and T_{ERK}), respectively, the quiescent cell acquires a proliferative advantage.

The cell cycle model in each tumor cell encompasses interactions among the concentrations of six components, denoted under brackets, and is given by the following system of ODEs [4]:

$$\frac{\text{d[CycB]}}{\text{d}t} = k_1 - (k_2^{'} + k_2^{''}\text{[Cdh1]} + \text{[p27/p21][HIF]})\text{[CycB]}, \tag{3}$$

$$\frac{\text{d[Cdh1]}}{\text{d}t} = \frac{(k_3^{'} + k_3^{''}\text{[p55cdc}_\text{A}\text{]})(1 - \text{[Cdh1]})}{J_3 + 1 - \text{[Cdh1]}} - \frac{k_4\text{[mass][CycB][Cdh1]}}{J_4 + \text{[Cdh1]}}, \tag{4}$$

$$\frac{\text{d[p55cdc}_\text{T}\text{]}}{\text{d}t} = k_5^{'} + k_5^{''}\frac{(\text{[CycB][mass]})^n}{J_5^n + (\text{[CycB][mass]})^n} - k_6\text{[p55cdc}_\text{T}\text{]}, \tag{5}$$

$$\frac{\text{d[p55cdc}_\text{A}\text{]}}{\text{d}t} = \frac{k_7\text{[Plk1]}(\text{[p55cdc}_\text{T}\text{]} - \text{[p55cdc}_\text{A}\text{]})}{J_7 + \text{[p55cdc}_\text{T}\text{]} - \text{[p55cdc}_\text{A}\text{]}} - \frac{k_8\text{[Mad][p55cdc}_\text{A}\text{]}}{J_8 + \text{[p55cdc}_\text{A}\text{]}} - k_6\text{[p55cdc}_\text{A}\text{]}, \tag{6}$$

$$\frac{\text{d[Plk1]}}{\text{d}t} = k_9\text{[mass][CycB]}(1 - \text{[Plk1]}) - k_{10}\text{[Plk1]}, \tag{7}$$

$$\frac{\text{d[mass]}}{\text{d}t} = \mu\text{[mass]}\left(1 - \frac{\text{[mass]}}{m_*}\right). \tag{8}$$

When the CycB concentration exceeds a threshold [$\overline{\text{CycB}}$], the cell division process begins, and the cell mass is halved. The initial conditions and the parameter values used in this model are shown in Table 2, and a complete description of the parameters can be found in Powathil et al. [4].

Table 2. Initial conditions and parameter values of the cell cycle model [4].

Component	**Meaning**	**Initial condition**	**Rate constants** (h^{-1})	**Dimensioless constants**
[CycB]	Cdk-cyclin B complex	0.094	$k_1 = 0.12$, $k_2^{'} = 0.12$, $k_2^{''} = 4.5$, [p27/p21] $= 1.05$	$[\overline{\text{CycB}}] = 0.1$
[Cdh1]	APC-Cdh1 complex	0.998	$k_3^{'} = 3$, $k_3^{''} = 30$, $k_4 = 105$	$J_3 = 0.04$, $J_4 = 0.04$
[p55cdc$_\text{T}$]	Total p55cdc-APC complex	0.998	$k_5^{'} = 0.015$, $k_5^{''} = 0.6$, $k_6 = 0.3$	$J_5 = 0.3$, $n = 4$
[p55cdc$_\text{A}$]	Active form of the p55cdc-APC complex	0.876	$k_7 = 3$, $k_8 = 1.5$	$J_7 = 0.001$, $J_8 = 0.001$, [Mad] $= 1$
[Plk1]	Active form of the Plk1 protein	0.574	$k_9 = 0.3$, $k_{10} = 0.06$	–
[mass]	Cell mass	0.452	$\mu = \mu^+ + \varepsilon\hat{\mu}$, $\mu^+ = 0.03$, $\hat{\mu} \sim \mathcal{U}[-1, 1]$	$m_* = 10$, $\varepsilon = 0.006$

2.3 The Cellular Scale

The cellular scale is represented by an agent-based model, which allows us to analyze each agent individually and describe its behavior in the microenvironment. An agent can interact with other agents and the microenvironment through different forces, which define the agent movement. We consider both healthy (normal) and cancer cells, and a pre-existing set of blood vessel cross-sections as agents. We assume that these blood vessel cross-sections are randomly distributed throughout the domain and remain spatially fixed during the simulation time. Blood vessels act as sources of oxygen and are responsible for delivering chemotherapeutic drugs. Cell morphology and properties are defined as in Rocha et al. [3]. Cell movement is governed by the balance of the following forces among cells, the blood vessels, and the microenvironment: cell–cell adhesion and cell–cell repulsion forces, blood vessel–cell adhesion and blood vessel–cell repulsion forces, compression and resistance to compression forces, and drag force of interstitial fluid flow (see Rocha et al. [7] for details).

Normal cells are kept in homeostasis, uptaking a small percentage of the oxygen present in the microenvironment. Tumor cells are differentiated into seven phenotypic states: quiescent ($\mathcal{Q}$), with positive proliferation stimulus ($\mathcal{P}_+$), with negative proliferation stimulus ($\mathcal{P}_-$), hypoxic ($\mathcal{H}$), necrotic ($\mathcal{N}$), apoptotic ($\mathcal{A}$), and killed by chemotherapy ($\mathcal{K}$). Such phenotypic differentiation is driven by interactions with the microenvironment and with other cells and intracellular regulatory responses. Transitions from quiescent ($\mathcal{Q}$) to proliferative ($\mathcal{P}_+$) or apoptotic ($\mathcal{A}$) states and from proliferative ($\mathcal{P}_+$ and $\mathcal{P}_-$) to drug-induced death ($\mathcal{K}$) state are stochastic and defined by the following Poisson processes [3, 5], given a time interval Δt:

$$\begin{aligned}
&P(\mathcal{P}_+|\mathcal{Q}) = 1 - \exp\left(-\alpha_P \Delta t\right), && \alpha_P(t) = \overline{\alpha}_P \left(\tfrac{K-\overline{K}}{1-\overline{K}}\right),\\
&P(\mathcal{A}|\mathcal{Q}) = 1 - \exp\left(-\alpha_A \Delta t\right), && \alpha_A = \text{constant},\\
&P(\mathcal{K}|\mathcal{P}_+) = 1 - \exp\left(-\alpha_{K_+} \Delta t\right), && \alpha_{K_+}(t) = \overline{\alpha}_{K_+} \left(\tfrac{C_t-\overline{C}}{1-\overline{C}}\right),\\
&P(\mathcal{K}|\mathcal{P}_-) = 1 - \exp\left(-\alpha_{K_-} \Delta t\right), && \alpha_{K_-}(t) = \overline{\alpha}_{K_-} \left(\tfrac{C_c-\overline{C}}{1-\overline{C}}\right).
\end{aligned} \tag{9}$$

The biochemical reactions of the EGFR signaling pathway determine $\overline{\alpha}_P$ depending on [ERK] and [PLC$_\gamma$] as well as on the [CycB] from the cell cycle signaling pathway according to the following rule:

$$\overline{\alpha}_P = 1, \text{ if } \frac{\text{d[PLC}_\gamma\text{]}}{\text{d}t} < T_{\text{PLC}}, \frac{\text{d[ERK]}}{\text{d}t} > T_{\text{ERK}}, \text{ and [CycB]} > [\overline{\text{CycB}}] \quad \text{or} \quad \overline{\alpha}_P = 0, \text{ otherwise.} \tag{10}$$

Similarly, parameters $\overline{\alpha}_{K_+}$ and $\overline{\alpha}_{K_-}$ depend on the drug concentration uptaken by the cell from a minimum quantity $\overline{C}$ accumulated by the cell according to the following rule:

$$\overline{\alpha}_{K_+} = 1, \text{ if } C_t(x,t) > \overline{C} \text{ and S-G2-M-phase of the cell cycle} \quad \text{or} \quad \overline{\alpha}_{K_+} = 0, \text{ otherwise,} \tag{11}$$

$$\overline{\alpha}_{K_-} = 1, \text{ if } C_c(x,t) > \overline{C} \text{ and G1-phase of the cell cycle} \quad \text{or} \quad \overline{\alpha}_{K_-} = 0, \text{ otherwise.} \tag{12}$$

Also notice that transitions from quiescent ($\mathcal{Q}$) and proliferative ($\mathcal{P}_+$ and $\mathcal{P}_-$) to hypoxic ($\mathcal{H}$) occur when the oxygen availability in the microenvironment is less than the threshold $\overline{K}$. Eventually, hypoxic cells die and become necrotic ($\mathcal{N}$). Other deterministic transitions depend only on the time elapsed from the state in which the cell is. Figure 2 illustrates the color scheme used to represent agents and their transitions.

Remark: All PDEs and systems of ODEs are numerically solved using the finite difference and the fourth-order Runge-Kutta methods [8], respectively. The discretization settings are chosen so that convergent solutions are obtained.

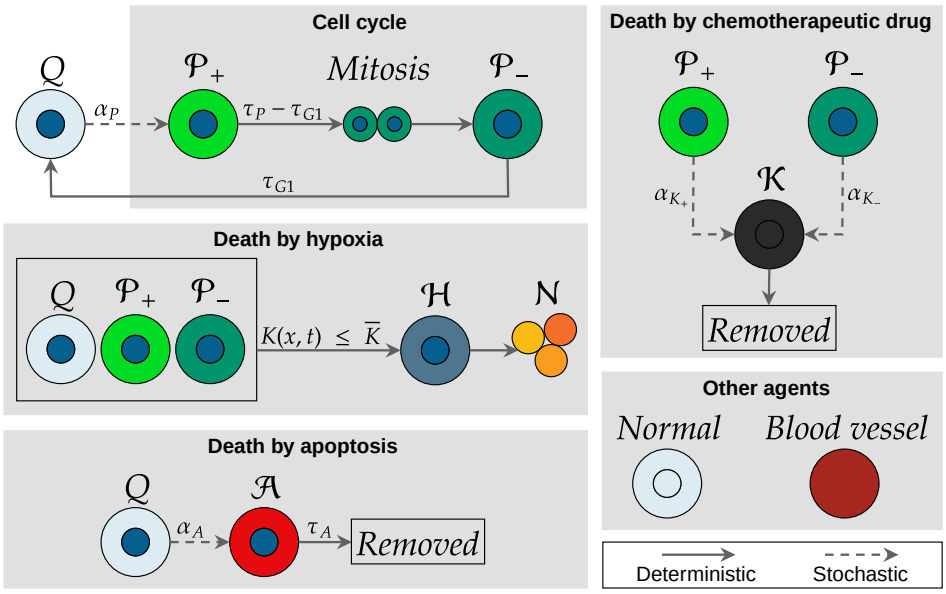

Figure 2. Schematic representation of normal cells, blood vessel cross-sections, and phenotypic differentiation of tumor cells and their transitions.

3 Results and Discussions

In the numerical experiments, we consider a 500×500 μm^2 computational domain for the tissue scale. At the cellular scale, normal and tumor cells and blood vessel cross-sections are arranged in a circular domain of radius equal to 250 μm inscribed in the macroscopic domain. The initial ABM condition consists of 759 agents: 32 blood vessel cross-sections, 723 normal cells, and four tumor cells (two quiescent cells and two cells with positive proliferation stimulus) that are placed close to the center of the domain. *In silico* experiments are performed up to the maximum time ($t_{\max}$) of 700 h. To analyze the effects on the dynamics of the injection of two chemotherapeutic drugs, in isolation, we conduct three experiments: the first one is the control experiment, in which no drug is applied during the whole simulation time; in the second experiment, the chemotherapeutic drug *cisplatin*, specific to the G1-phase of the cell cycle, is injected at $t = 400$ h; and in the last experiment, we introduce the drug *taxotere*, specific to the S-G2-M-phases of the cell cycle, also at $t = 400$ h.

Figure 3 illustrates the dynamics of tumor growth without the application of chemotherapeutic drugs. Snapshots of one realization of the ABM are shown every 100 h, from $t = 200$ h to $t = 700$ h, using the color scheme represented in Figure 2. Tumor cells, initially located in the center of the domain, begin to proliferate closer to regions where there is greater oxygen availability (closer to the blood vessels). However, as the tumor grows, the oxygen demand increases, followed by the consequent decrease in its availability. The onset of hypoxic cells is around $t = 200$ h, and clusters of necrotic cells are well-formed at $t = 300$ h. The number of necrotic cells significantly increases over time. At the final simulation time ($t_{\max} = 700$ h), the tumor completely occupies the circular domain. We also notice that the quiescent and proliferative cells are closer to the blood vessels; on the other hand, necrotic cells are mostly arranged in other regions of the domain.

Figure 4 illustrates one realization of tumor dynamics subject to the injection of one dose of *cisplatin* at time $t = 400$ h, which induces the death of tumor cells that have negative proliferation stimulus ($\mathcal{P}_-$). The drug effects are seen at time $t = 500$ h when regions with no agents appear caused by death due to chemotherapy. However, because *cisplatin* has a relatively high diffusion coefficient and decay rate, killing effects on tumor cells quickly vanish. At the final simulation time, tumor cells proliferate again and occupy a large part of the circular domain.

Figure 5 illustrates one realization of tumor dynamics subject to the injection of one dose of *taxotere* at time $t = 400$ h, which acts by killing tumor cells that have positive proliferation stimulus ($\mathcal{P}_+$). At time $t = 500$ h, we can notice the existence of empty regions caused by cells killed by the chemotherapy. Since *taxotere* has a lower diffusion coefficient and decay rate compared to *cisplatin*, the chemotherapy effect is kept until the final simulation time ($t_{\max} = 700$ h). At this time, only quiescent and necrotic tumor cells remain in the circular domain, and the effects of the S-G2-M-specific drug prevent proliferation from quiescent cells. Thus, as long as there is a considerable drug concentration in the microenvironment, tumor growth remains inactive. However, since quiescent cells are living cells in a state of dormancy, the tumor evolution can be reestablished at a later time.

Figure 6 illustrates the time evolution of the number of tumor cells considering 10 realizations for each *in*

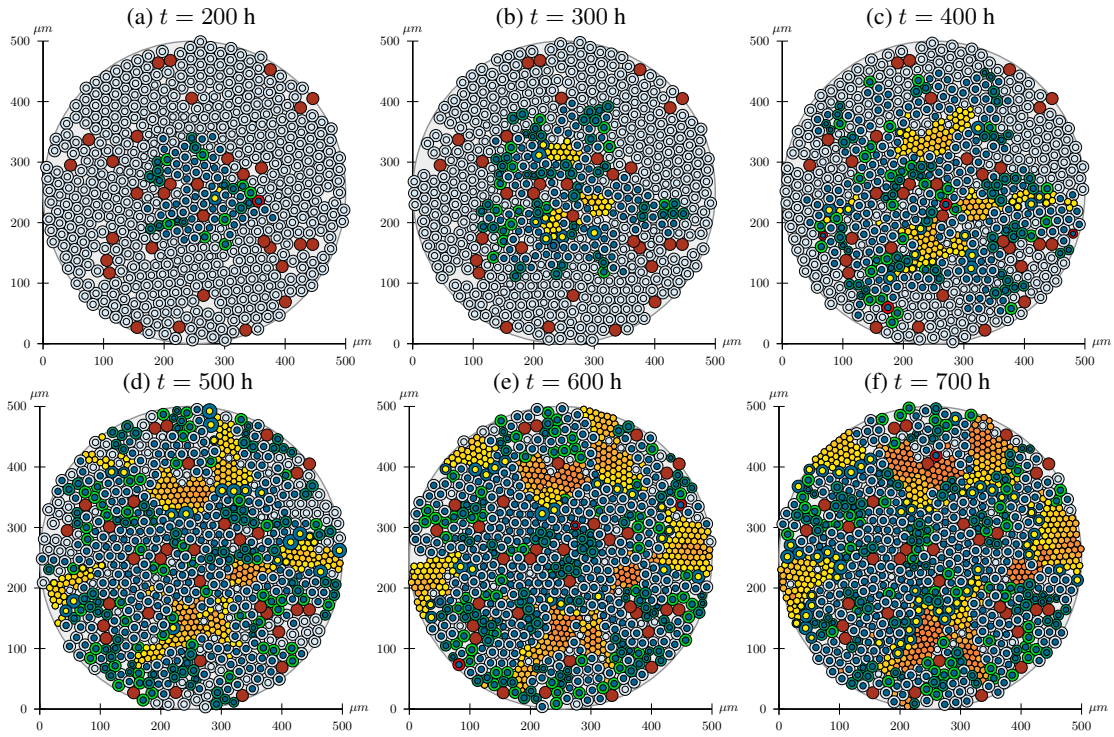

Figure 3. Dynamics of tumor growth without application of chemotherapeutic drugs.

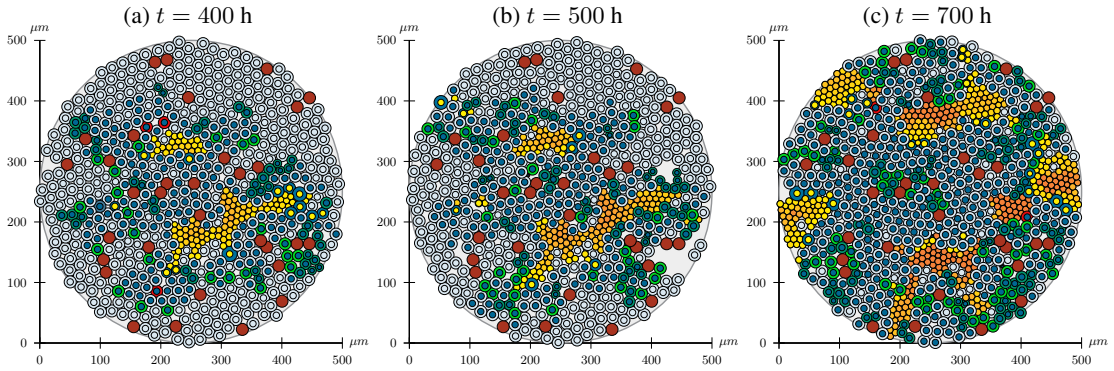

Figure 4. Dynamics of tumor growth with application of the drug *cisplatin* in one dose.

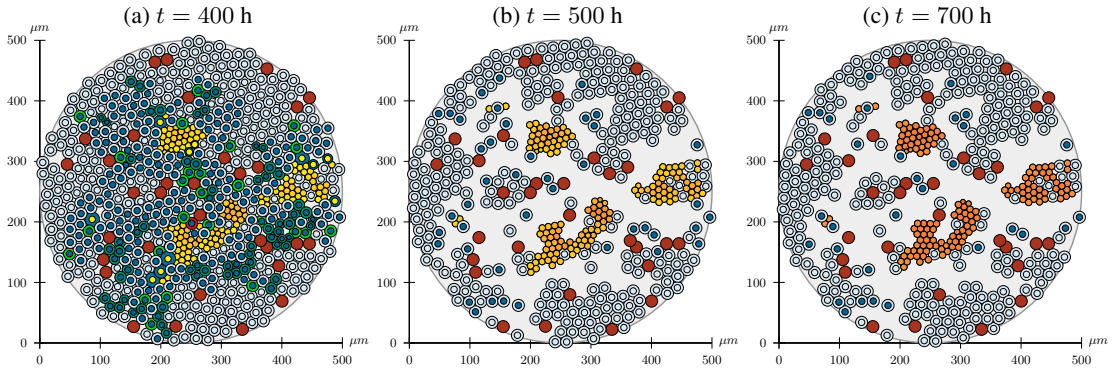

Figure 5. Dynamics of tumor growth with application of the drug *taxotere* in one dose.

silico experiment. We present the number of necrotic ($\mathcal{N}$), quiescent ($\mathcal{Q}$), with positive proliferation stimulus ($\mathcal{P}_+$), and with negative proliferation stimulus ($\mathcal{P}_-$) cells until the final simulation time. This figure provides another view of the dynamics of tumor growth and shows the effectiveness of *taxotere* compared to *cisplatin*. While with *cisplatin* an average of 300 quiescent cells remain in the computational domain at the end of the simulation, chemotherapy with *taxotere* reduces this number to less than half and manages to eliminate proliferative tumor cells.

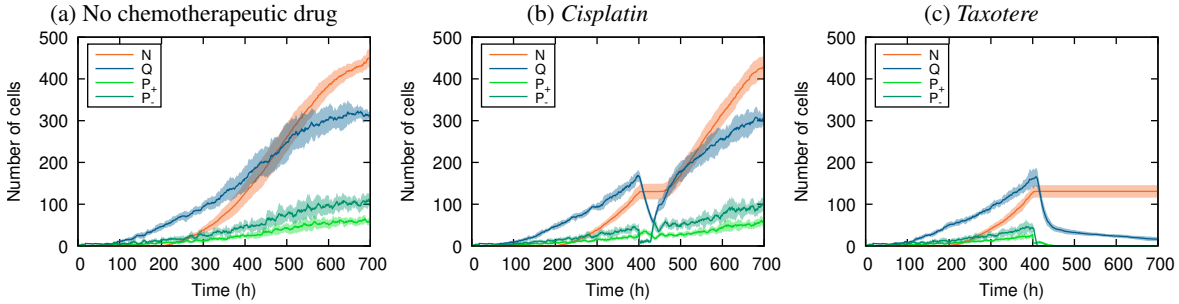

Figure 6. Mean evolution of the number of tumor cells and standard deviation over time.

4 Conclusion

The developed hybrid multiscale model integrates characteristics present at three scales: tissue, cellular, and intracellular. The multiscale approach makes the tumor growth modeling biologically more relevant, providing a better description of the phenomena separately. In addition, the modular framework of this approach allows us to easily include and change features in the model. The *in silico* experiments carried out showed that the injection of one dose of two different chemotherapeutic drugs, in isolation, is not able to completely eliminate the tumor. In addition to the different forms of action on the cell cycle, drug diffusion coefficient and decay rate also ultimately play an important role in chemotherapy effectiveness. Overall, the developed model allows investigating the effects of phase-specific chemotherapeutic drugs, drug combinations, and different treatment protocols. Although not shown, combination with targeted inhibitors, such as EGFR-inhibiting drugs, can be also studied through simulations. In this way, it can be used as an initial platform for studying and incorporating specific treatment features, such as drug resistance, targeted therapies, and optimal treatment control.

Acknowledgements. The authors would like to thank *Fundação de Amparo à Pesquisa do Estado do Rio de Janeiro* (FAPERJ) and *Coordenação de Aperfeiçoamento de Pessoal de Nível Superior* (CAPES) for financial support.

Authorship statement. The authors hereby confirm that they are the sole liable persons responsible for the authorship of this work, and that all material that has been herein included as part of the present paper is either the property (and authorship) of the authors, or has the permission of the owners to be included here.

References

[1] Wang, Z., Butner, J. D., Kerketta, R., Cristini, V., & Deisboeck, T. S., 2015. Simulating cancer growth with multiscale agent-based modeling. *Seminars in Cancer Biology*, vol. 30, pp. 70 – 78. Cancer modeling and network biology.

[2] Chamseddine, I. M. & Rejniak, K. A., 2020. Hybrid modeling frameworks of tumor development and treatment. *WIREs Systems Biology and Medicine*, vol. 12, n. 1, pp. e1461.

[3] Rocha, H. L., Almeida, R. C., Lima, E. A. B. F., Resende, A. C. M., Oden, J. T., & Yankeelov, T. E., 2018. A hybrid three-scale model of tumor growth. *Mathematical Models and Methods in Applied Sciences*, vol. 28, n. 01, pp. 61–93.

[4] Powathil, G. G., Gordon, K. E., Hill, L. A., & Chaplain, M. A., 2012. Modelling the effects of cell-cycle heterogeneity on the response of a solid tumour to chemotherapy: Biological insights from a hybrid multiscale cellular automaton model. *Journal of Theoretical Biology*, vol. 308, pp. 1 – 19.

[5] Macklin, P., Edgerton, M. E., Thompson, A. M., & Cristini, V., 2012. Patient-calibrated agent-based modelling of ductal carcinoma in situ (DCIS): From microscopic measurements to macroscopic predictions of clinical progression. *Journal of Theoretical Biology*, vol. 301, pp. 122 – 140.

[6] Hamis, S., Nithiarasu, P., & Powathil, G. G., 2018. What does not kill a tumour may make it stronger: In silico insights into chemotherapeutic drug resistance. *Journal of Theoretical Biology*, vol. 454, pp. 253 – 267.

[7] Rocha, H. L., Almeida, R. C., & Lima, E. A. B. F., 2017. Um modelo híbrido para o crescimento tumoral vascular. In *Proceedings of the XXXVIII Ibero-Latin American Congress on Computational Methods in Engineering (CILAMCE)*, Florianópolis - SC, Brazil.

[8] LeVeque, R. J., 2007. *Finite Difference Methods for Ordinary and Partial Differential Equations*. Society for Industrial and Applied Mathematics.